Bioorganic Chemistry 69 (2016) 140–152

Contents lists available at ScienceDirect

Bioorganic Chemistry

journal homepage: www.elsevier.com/locate/bioorg

Some new nano-sized Fe(II), Cd(II) and Zn(II) Schiff base complexes as precursor for metal oxides: Sonochemical synthesis, characterization, DNA interaction, *in vitro* antimicrobial and anticancer activities

Laila H. Abdel-Rahman, Ahmed M. Abu-Dief *, Rafat M. El-Khatib, Shimaa Mahdy Abdel-Fatah

Chemistry Department, Faculty of Science, Sohag University, 82534 Sohag, Egypt

ARTICLE INFO

Article history:
Received 9 July 2016
Revised 6 September 2016
Accepted 30 October 2016
Available online 1 November 2016

Keywords:
DNA interaction
Antimicrobial activity
Nanoparticles
Metal oxides
Cytotoxic activity

ABSTRACT

The complexes of Fe(II), Cd(II) and Zn(II) with Schiff base derived from 2-amino-3-hydroxypyridine and 3-methoxysalicylaldehyde have been prepared. Melting points, decomposition temperatures, Elemental analyses, TGA, conductance measurements, infrared (IR) and UV–Visible spectrophotometric studies were utilized in characterizing the compounds. The UV–Visible spectrophotometric analysis revealed 1:1 (metal-ligand) stoichiometry for the three complexes. In addition to, the prepared complexes have been used as precursors for preparing their corresponding metal oxides nanoparticles via thermal decomposition. The structures of the nano-sized complexes and their metal oxides were characterized by X-ray powder diffraction and transmittance electron microscopy. Moreover, the prepared Schiff base ligand, its complexes and their corresponding nano-sized metal oxides have been screened *in vitro* for their antibacterial activity against three bacteria, gram-positive (*Micrococcus luteus*) and gram-negative (*Escherichia coli*, *Serratia marcescence*) and three strains of fungus. The metal chelates were shown to possess more antimicrobial activity than the free Schiff-base chelate and their nano-sized metal oxides have the highest activity. The binding behaviors of the complexes to calf thymus DNA have been investigated by absorption spectra, viscosity mensuration and gel electrophoresis. The DNA binding constants reveal that all these complexes interact with DNA through intercalative binding mode. Furthermore, the cytotoxic activity of the prepared Schiff base complexes on human colon carcinoma cells, (HCT-116 cell line) and hepatic cellular carcinoma cells, (HepG-2) showed potent cytotoxicity effect against growth of carcinoma cells compared to the clinically used Vinblastine standard.

1. Introduction

Transition metal complexes derived from the Schiff base ligands with biological potency have been widely studied. Schiff bases appear to be an important intermediate in a number of enzymatic reactions including interaction of an enzyme with an amino or a carbonyl group of the substrate. One of the most important kinds of catalytic mechanism is the biochemical process which involves the condensation of a primary amine in an enzyme that of a lysine residue, with a carbonyl group of the substrate to form Schiff base [1]. Transition metal complexes with different oxidation states have a strong role in bioinorganic chemistry and may offer the basis of models for active sites of biological systems [2,3]. On the other hand, ZnO NPs are of particular interest because they can be prepared easily cheap and secure matter for human beings and animals. They are extensively utilized in the formulation of healthcare products [4]. It has long been identified as a serious co-factor in biological compounds, either as a compositional template in protein folding or as a Lewis acid catalyst which can readily adopt the coordination numbers 4, 5, or 6 [5,6]. There is substantial importance in the coordination chemistry of cadmium complexes as a result of the toxic environmental effect of cadmium. The mobilization and immobilization of cadmium in the climate, in organisms, and in some technical systems (such as in ligand exchange chromatography) have been presented to depend manifestly on the complexation of the metal center by chelating nitrogen donor ligands [7]. The size and shape of the nanomaterials are key factors for shaping their characteristics such as, electrical, optical, magnetic, antimicrobial and catalytic potency. Metal and metal oxide nanoparticles have found wide diversity of uses, including heterogeneous catalysts, environmental remediation, electronic, chemical sensing devices, medicinal fields, separations, thin films, inks, disinfection, and antimicrobial

* Corresponding author.
E-mail address: ahmed_benzoic@yahoo.com (A.M. Abu-Dief).

http://dx.doi.org/10.1016/j.bioorg.2016.10.009
0045-2068/

activity [8]. The different applications of metal and metal oxide nanoparticles altered with morphology and size [9]. The detection of metal ions of biological importance has attracted much attention. Zn^{2+} ion fluorescent probes or sensors have achieved special interest. Zn^{2+} is an essential trace element and the second most abundant metal ion in humans (after Fe^{2+}) [10]. Thus, the present aim of the work is to synthesize a Schiff base derived from 2-amino-3-hydroxypyridine and 3-methoxysalicylaldehyde and to prepare its transition metal complexes, characterize them and inspect their antibacterial, antifungal and anticancer activities. We also studied their interaction with DNA. Nano-sized particles of that complexes and their corresponding metal oxides nanoparticles also were prepared. We also investigate the antimicrobial activity of the prepared metal oxides nanoparticles.

2. Experimental

All the starting matters of chemicals used in this investigation Such as 3-methoxysalicylaldehyde (v), 2-amino-3-hydroxypyridine (ahp), the metal salts ($FeSO_4$. $(NH_4)_2SO_4{\cdot}6H_2O$, $Zn(NO_3)_2{\cdot}6H_2O$, $Cd(NO_3)_2{\cdot}4H_2O$), Calf thymus DNA (CT-DNA), bromophenol blue dye, ethidium bromide and Tris[hydroxymethyl]-aminomethane (Tris) were acquired from Sigma–Aldrich Chemie (Germany). Spectroscopic degree ethanol, dimethylformamide (DMF) and HCl products were used.

2.1. Synthesis of Schiff base ligand

An equimolar mixture of 2-amino-3-hydroxypyridine (0.110 g, 1 mmol) and 3-methoxysalicylaldehyde (0.152 g, 1 mmol) dissolved in 10 ml ethyl alcohol and mixture was refluxed for 1 h. The reaction mixture was filtered, rinsed with water and recrystallised from ethanol. The Schiff base was dried under reduced pressure in a desiccator. The purity of prepared compounds was checked by TLC utilizing silica gel G (yield: 88%) as shown in (cf. Scheme 1):

^{1}H NMR (δ, ppm), in DMSO: (6.85–8.00 (m, 6H-Ar), 9.44 (s, 1H, CH = N), 10.28 (s, 1H, OH), 3.34 (s, 3H, OCH_3)).

^{13}C NMR (δ, ppm), in DMSO: 166 (CH = N), 155, 150, 149, 144, 143, 125, 124, 123, 122, 120, 118 (11CH-Ar), 56 (OCH_3).

2.2. Preparation of complexes with nano-structures by sonochemical route

10 ml of a 0.1 M (1 mmol) solution of metal salt [($FeSO_4$.$(NH_4)_2$-$SO_4{\cdot}6H_2O$, 0.392 g), ($Zn(NO_3)_2{\cdot}6H_2O$, 0.297 g), ($Cd(NO_3)_2{\cdot}4H_2O$, 0.308 g)] in Ethanol was positioned in a high-density ultrasonic probe, elaborating at 24 kHz with a maximum power output of 400 W. Into this solution, 10 ml of a 0.1 M solution of the ligand (ahpv) (0.260 g, 1 mmol) was added drop wise. The acquired precipitate was filtered off, rinsed with ethanol and then dried in air as shown in (cf. Scheme 2):

^{1}H NMR (δ, ppm), in DMSO: (ahpvCd: 6.45–7.40 (m, 6H-Ar), 9.20 (s, 1H, CH = N), 3.79 (s, 3H, OCH_3); ahpvZn: 6.42–7.51 (m, 6H-Ar), 9.26 (s, 1H, CH = N), 3.77 (s, 3H, OCH_3)).

2.3. Synthesis of metal oxide nano particles

Nano-sized metal oxides were prepared by calcination of (0.05 g) of complexes with nano-structures in air at 500 °C with heating rate 10 °C min^{-1}. The structures of the nano-sized oxides or metals were identified by transmmitance electron microscopy and X-ray powder diffraction.

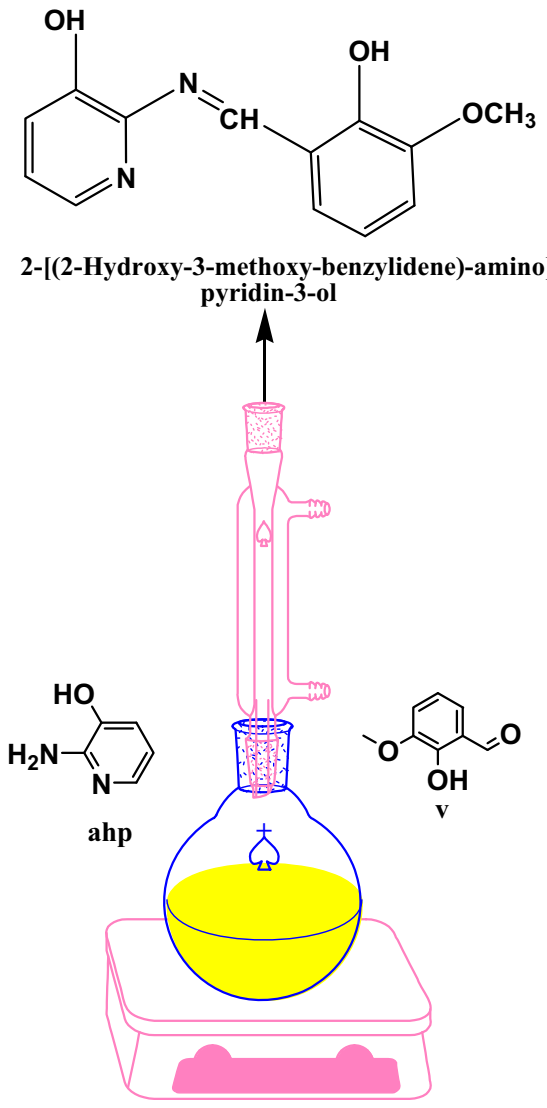

Scheme 1. Synthesis of Schiff base ligand (ahpv), where ahp = 2-amino-3-hydroxypyridine and v = 3-methoxysalicylaldehyde (o-vanillin).

2.4. Physical measurements

Melting point for Schiff base and decomposition points for complexes were carried out on a melting point apparatus, Gallenkamp, UK. IR spectra of the metal complexes in KBr powder in the range of 4000–400 cm^{-1} were recorded making use of Shimadzu FTIR model 8101 spectrophotometer. Molar conductivity measurements were made by using JENWAY conductivity meter model 4320 at 298 K using DMF as solvent. UV–visible spectra in DMF were registered utilizing 10 mm matched quartz cells on PG spectrophotometer model T + 80. ^{1}H NMR and ^{13}C NMR spectra were carried out in DMSO on BRUKER model 400 MHz using TMS as an internal standard (δ ppm) and DMSO-d_6 as the solvent. The Schiff base and their complexes were conquered to elemental analyses which was made at the analytic unit of the central lab of Cairo University by Elemental analyzer Perkin-Elmer model 240c. The magnetic measures were performed on Gouy's balance and the diamagnetic correction was made by Pascal's constants. Thermo gravimetric test was made under N_2 conditions with a warming rate 10 °C min^{-1} on Shimaduz corporation 60H analyzer. The values of absorbance of 1×10^{-3} M of each complex were measured at various PH levels. The pH levels were checked by using a series

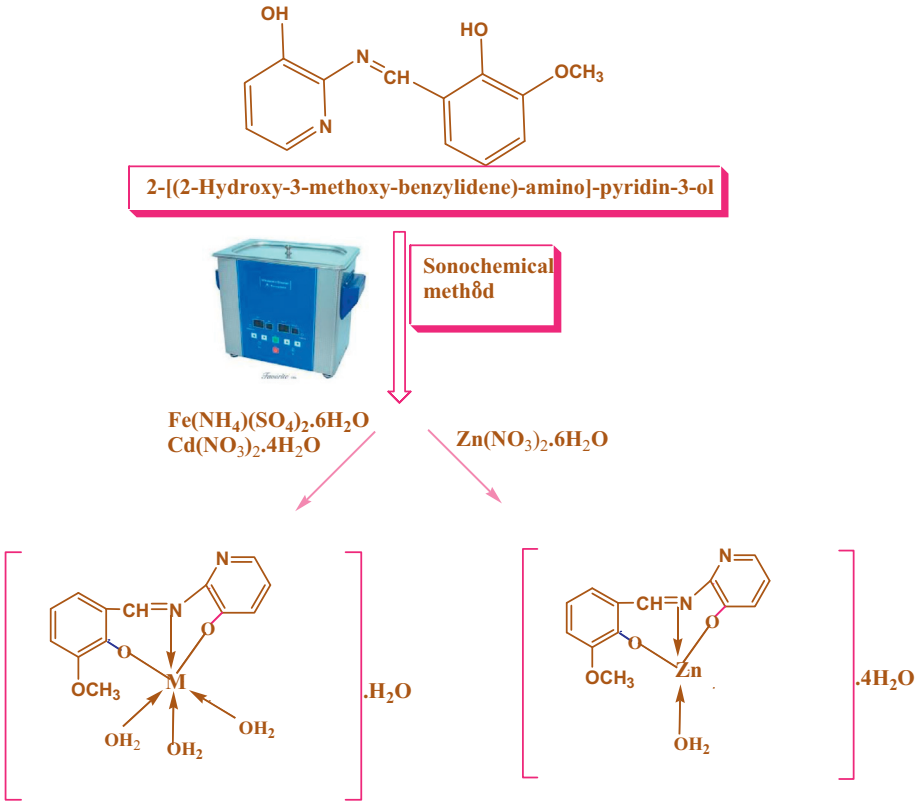

Scheme 2. The suggested structures of ahpvFe, ahpvCd, ahpvZn complexes: for ahpvFe and ahpvCd complexes: n = 1 and ahpvZn complex: n = 4.

of Britton universal buffers [11]. pH measurements were made using HANNA 211 pH meter at 298 ± 1 K. TEM images were recorded using transmittance electron microscope (TEM-2100), Faculty of Science, Alex. University. An ultrasonic generator (Dr. Hielscher UP400 S ultrasonic processor) elaporated with an "H22" sonotrode with diameter 22 mm, working at 24 kHz with a maximum force output of 400 W, was utilized for the ultrasonic irradiation. The chemical composition of the synthesized nanostructures was also analyzed using energy dispersive analysis of X-ray (EDAX) unit. X-ray powder diffraction (XRD) gauges were performed using a Philips diffractometer made by X'pert with monochromatized Cu Kα radiation. Particle size distribution of the prepared imine complexes and their corresponding metal oxides was evaluated using image J Launcher, broken-symmetry software, version (1.4.3.6.7).

2.5. Antimicrobial activity

The *in vitro* biological screening activities of the investigated compounds were examined against the gram negative bacteria *(Escherichia coli* and *Serratia marcescence)* and gram positive bacteria *(Micrococcus luteus) by* the well diffusion route using agar nutrient as the medium. While antifungal effect was carried out using potato Dextrose Agar as medium against *(Getrichm candidum, Aspergillus flavus and Fusarium oxysporum*). The stock solutions were made ready by dissolving the compounds in DMF. In a typical process, a well was made with the help of borer on the nutrient medium plate which was formerly inoculated with microorganisms. The well was made full with the various concentrations of test solution using a micropipette and incubated at 37 °C for 24 h (bacteria) and 48 h (fungus). Ofloxacin and Fluconazol were used as standard against the bacteria and fungi respectively. During incubation time, the test solution transpired and the growth of the inoculated microorganisms was affected. Antimicrobial activity was indicated by the presence of obvious zone of inhibition around the wells. The zone of inhibition was evaluated in mm [12]. The preparation of metal oxides followed this route: First of all, Petri plates were made by (20 ml) of sterile Muller Hinton Agar for bacteria and (20 ml) of potato Dextrose Agar in case of yeast [13]. The 24 h prepared test cultures of inoculums were swabbed on the top of the sclerotic media and left to dry for 10 min. Previously prepared metal oxides nanoparticles impregnated nipping at the different concentrations of 10 and 20 (mg/ml) for bacteria and fungi were placed aseptically on sensitivity plates with suitable controls. The loaded discs were put on the surface of the medium and left for 30 min at room temperature for compound diffusion. Ofloxacin was used as positive control for bacteria and Fluconazol was utilized as positive control for fungi. After that all the plates were incubated for 24 h at 37 °C for bacteria and 28–35 °C for fungi, respectively. The sensibility was registered by measuring the clear zone of growth inhibition of agar surface around the discs in millimeter.

2.6. DNA binding experiments

All the experiments including the interaction of the complexes with DNA were performed in Tris–HCl buffer (55 mM, pH 7.4). CT-DNA was purified by centrifugal dialysis before utilization. A solution of calf thymus DNA in the buffer presented a ratio of UV absorbance at 260 and 280 nm of about >1.87, indicating that the DNA was sufficiently free from protein contamination [14]. The concentration of DNA was estimated by monitoring the UV absorbance at 260 nm using $\varepsilon_{260} = 6600\ mol^{-1}\ cm^2$. The stock solution was saved at 5 °C and used within only two days.

2.6.1. Absorption spectral studies

Absorption spectral studies were carried out in (55 mM Tris-HCl buffer, pH 7.4) buffer at room temperature to investigate the binding affinity between CT - DNA and complex. The concentration of CT - DNA was checked from the absorption intensity at 260 nm with a ε value of 6600 mol^{-1} cm^2. Absorption titration experiments were performed by altering the concentration of the CT - DNA (0–30 μM) keeping the complex concentration (10^{-3} M) as constant. The absorbance (A) was registered after each addition of CT - DNA. The stock solution was stored at 5 °C and used within only two days. In order to remove the absorbance of the CT-DNA an equal amount of the same was added to both the compound solution and the reference solution. The intrinsic binding constant, Kb for the complexes was determined from the spectral experiments data using the following equation [15]:

$$\frac{[DNA]}{(\varepsilon_a - \varepsilon_f)} = \frac{[DNA]}{(\varepsilon_b - \varepsilon_f)} + \frac{1}{[K_b(\varepsilon_b - \varepsilon_f)]} \quad (1)$$

Here, ε_a, ε_f, and ε_b are apparent, free and fully bound complex extinction coefficients respectively, where; [DNA] is the concentration of DNA in base pairs. In particular, ε_f was evaluated from the calibration curve of the isolated metal complex; following the Beer's law. ε_a was rated as the ratio between the measured absorbance and the complex concentration, A_{obs}/[complex]. The data were suited to the above equation with a slope equal to $1/(\varepsilon_b - \varepsilon_f)$ and y-intercept equal to $1/[K_b(\varepsilon_b - \varepsilon_f)]$ and K_b was rated from the ratio of the slope to the intercept. The standard Gibbs free energy for DNA binding was evaluated from the following relation [16]:

$$\Delta G_b^{\neq} = -RT \ln K_b \quad (2)$$

2.6.2. Viscosity experiments for interaction of the prepared complexes with DNA

Viscosity measurements were made using an Oswald micro viscometer, kept at constant temperature at 25 ± 1 °C in thermostat. The fluidity times were recorded for various concentrations of the complex (10–60 μM), keeping the concentration of DNA constant (50 μM). Blending of the solution was made by bubbling the N_2 gas through the viscometer. The average value of the three measures was utilized to rate the viscosity of the samples. The buffer flow time in seconds was registered as t°. The relative viscosities for DNA in the presence (η) and disappearance (η°) of the complex were calculated by using the relation η = (t − t°)/t°. Where, t is the notified flow time in seconds and the values of the relative viscosity (η/η°) were plotted against 1/R (R = [DNA]/[Complex]) [17].

2.6.3. Agarose gel electrophoresis

The DNA binding experiment was conducted utilizing CT DNA by gel electrophoresis with the corresponding metal complex. The reaction mixture was incubated before electrophoresis experiment at 37 °C for 45 min as follows: CT DNA 25 μM, 60 μM each complex. The samples (mixed with bromophenol blue dye at a 1:1 ratio) were electrophoresed for 30 min at 60 V on 1% agarose gel using TBE buffer, pH = 8.1. After electrophoresis, the gel was stained utilizing 2 $\mu g/cm^3$ ethidium bromide (EB) and photographed under UV light using Lumix Digital camera [18].

2.7. Anticancer activity

The anticancer activity was made at the National Cancer Institute, Cancer Biology Department, Pharmacology Department, Cairo University. The absorbance or optical density (O.D.) of each well was evaluated spectrophotometrically at 564 (nm) with an "ELIZA" micro plate reader (Meter tech. Σ 960, "USA"). Estimation of the cytotoxic potency of the ligand and its complexes was carried out against Colon carcinoma cells, (HCT-116 cell line) and hepatic cellular carcinoma cells, (HepG-2). The evaluation process was carried out *in vitro* using the Sulfo-Rhodamine-B-stain (SRB) [19]. Cells were placed in 96-multiwell plate (10^4 cells/well) for 24 h before processing with the complexes to allow attachment of cell to the wall of the plate. Various concentrations of the compounds under check in DMSO (0, 1, 2.5, 5 and 10 μM) were added to the cell monolayer. Monolayer cells were incubated with the compounds for 48 h at 37 °C and in atmosphere of 5% CO_2. After 48 h, cells were fixed, rinsed, and stained with Sulfo-Rhodamine-B-stain. Excess stain was rinsed with acetic acid and attached stain was treated with Tris EDTA buffer. Color intensity was rated in an ELISA reader. IC_{50} was evaluated and potency was calculated with regard to percentage of alteration of (vistabline standard) [20,21].

3. Results and discussion

3.1. Physicochemical properties

All the compounds are tinted, solid and stable at room temperature. The Analytical and physical data of ligand and complexes are recorded in (Table 1). The metal complexes exhibit 1:1 (metal-ligand) stoichiometry.

3.2. ^{1}H NMR and ^{13}C NMR spectra of ligand and their diamagnetic complexes

The ^{1}H NMR spectra of the L_1H ligand gives the signal at 6.85–8.00 (m) δ for aromatic proton and 9.44 (s) δ for azomethine proton. The peak at 10.28 (s) δ is due to —OH group, disappeared upon addition of D_2O. The peak at 3.34 (s) δ is due to —OCH_3 group. The ^{13}C NMR are offering the signals at various values of δ as follows: at δ 169 ppm (CH = N) due to azomethine and at δ 122–156 ppm (11CH-Ar) for aromatic carbon atoms [22]. Also at δ 56 ppm (OCH_3) due to carbon atom of methoxy group [23]. The ^{1}H NMR (DMSO-d_6, ppm) of ahpvCd and ahpvZn complexes shows singlet signal at 9.20 and 9.26 for CH = N protons respectively, multiple signals at 6.45–7.40 and 6.42–7.51 for six and six aromatic protons respectively, The ^{1}H NMR (DMSO-d_6, ppm) of ahpvCd and ahpvZn shows singlet signal at 3.79 and 3.77 for three OCH_3 protons. It is shown that the signal for OH protons is disappeared. This indicates happening of chelation of ligands with metal ions and deprotonating of —OH phenolic of pyridine and benzene ring. Also, the shift in signals for CH = N protons confirm chelation and deprotonating of phenolic —OH [23].

3.3. Infrared spectra

The IR spectra of the complexes were compared with those of the free ligands in order to determine the involvement of the coordination positions in the chelation. Characteristic peaks in the spectra of the ligand and complexes were considered and compared. IR spectrum of the ahpv ligand exhibited the most characteristic bands at 1613 cm^{-1} ν(C=N, azomethine) and 1307 cm^{-1} ν(C—O) [24]. The formation of the Schiff base was noted from the absence of C=O and NH_2 peaks in the ligand. The band at 1613 cm^{-1} due to the azomethine group of the Schiff base was shifted to lower frequencies (1593–1594 cm^{-1}) after complexation, indicating the bonding of nitrogen of the azomethine group to the metal ions. The phenolic C—O stretching vibration that appeared at 1307 cm^{-1} in Schiff base shifted towards lower frequencies in the complexes. This proposes deprotonation of the phenolic OH group after its chelation with the metal ion. The appearance of broad bands at around 3455–3468 cm^{-1} in the

Table 1
The analytical and physical data of ligand and its metal complexes.

Compound	Colour	(M. p) and Dec. p °C	M.wt	Elemental analysis found (calculated)			Conductance Λm (Ω^{-1} cm^2 mol^{-1})	μ_{eff} B.M.
				N	H	C		
ahpv	Orange	250	260	10.76 (10.64)	4.61 (4.71)	60.00 (60.15)	–	–
ahpvFe	Brown	295	369.8	7.57 (7.61)	4.86 (4.75)	42.18 (42.29)	33.7	4.95
ahpvCd	Yellow	>300	426.4	6.56 (6.60)	4.22 (4.33)	36.58 (36.43)	8.5	dia
ahpvZn	Orange	>300	397.38	7.04 (6.91)	5.03 (4.95)	39.25 (39.38)	13.15	dia

spectra of complexes may be due to water molecules [25–28]. A band of medium intensity at 967–977 cm^{-1} (OH rocking) suggests the presence of coordinated water in all three complexes. In the low frequency part, the band of weak intensity observed for the complexes in the region 516–580 cm^{-1} is attributed to M—O and in the region 417–517 cm^{-1} to M—N as shown in Table S1.

3.4. Electronic spectra

The nature of the ligand field around the metal ion was derived from the electronic spectra. The electronic absorption spectra of ligands and their complexes were on record at the wavelength range 800–200 nm and at 298 K. The ligand exhibits absorption bands in UV–Vis region around 355 nm which is specified to $n \rightarrow \pi^*$ transition originating from the azo methane function of the Schiff base ligand [29]. The absorption bands of complexes at λ_{max} = 390–449 nm is assigned to charge transfer with in Schiff base ligands [30]. Furthermore, A long and a broad band lying in the region 531 nm (ε_{max} = 110 mol^{-1} $cm^{2)}$. This band could be mainly attributed to the d → d transition in the structure of ahvpFe complex [31] as shown in (Fig. S1). It is was shown that no d-d transition in ahvpCd and ahvpZn complexes because it contains a full d subshell.

3.5. Magnetic moment measurements

The paramagnetic compounds will be attracted while the diamagnetic compounds repelled in a magnetic field. Therefore, paramagnetic substances will have positive susceptibilities. Thus, the magnetic susceptibility measures determine geometry of the complexes. Magnetic susceptibility measurements showed that Fe(II) complexes has paramagnetic character with octahedral geometry [32], but Cd(II) and Zn(II) complexes has diamagnetic character with octahedral with tetrahedral geometry, respectively [33].

3.6. Thermal analysis

Thermo gravimetric test was made under N_2 with a heating rate of 10 °C min^{-1}. The ahpvFe, ahpvCd and ahpvZn complexes have weight losses of 4.74, 3.35 and 18.12%, respectively, which are due to abstraction of water molecules of hydration. The weight losses of 23.08, 31.50 and 25.00% corresponding to the abstraction of the remaining thermally degradable part of the complex at temperature range 169.5–510.1 °C with respect to ahpvFe complex. The weight casualties of 23.57, 17.39, 6.61 and 21.65% corresponding to the elimination of the residual thermally degradable part of the complex at temperature range 142.4–528.3 °C with respect to ahpvCd complex. The weight losses of 34.63 and 30.85% corresponding to the elimination of the remaining thermally degradable part of the complex at temperature range 188.6–526.1 °C with respect to ahpvZn complex as shown in (Table S2). The weight losses of 37.75 and 15.71% [34]. The final product explained from a horizontal curve has been obtained suggesting formation of metal product [35].

3.7. Kinetic aspects

The thermodynamic parameters of the degradation processes of the complexes were calculated using the Coasts-Red fern equation [36],

$$\log\left[\frac{\log(w_\infty - w))}{T^2}\right] = \log\left[\frac{AR}{\phi E^*}\left(1 - \frac{2RT}{E^*}\right)\right] - \frac{E^*}{2.303RT} \quad (3)$$

where W_∞ is the mass loss at the completion of the decay reaction. W is the mass perishing up to temperature T, R is the gas constant and ϕ is the heating rate. Since 1-2RT/E^* ≈1, the plot of the left hand of equation against 1/T would give a straight line. E^* was then estimated to form the slope and the Arrhenius constant, A, was acquired from the intercept. The other kinetic parameters; the entropy of activation (S^*), enthalpy of energizing (H^*) and the free energy variance of activation (G^*) were calculated using the following equations:

$$S^* = 2.303R \log\frac{Ah}{kT} \quad (4)$$

$$H^* = E^* - RT \quad (5)$$

$$G^* = H^* - TS^* \quad (6)$$

where (k) and (h) are Boltzmann's and Plank's invariables, respectively. The kinetic parameters are listed in (Table S3). It is shown that G^* values increase due to increasing temperature. The positive values of H^* dissect that degradation processes are endothermic. In most thermal steps, S^* values are negative submitting a decomposition via abnormal pathway at those steps and the degradation processes are unfavorable. The negative activation entropy value slices that the activated complexes were more ordered than the reactant and that the reactions were slow. The more ordered nature was attributed to the polarization of bonds in the activated state, which might take place through charge transfer electronic transitions. Finally, positive values were found for H^* and G^* respectively symbolizing endothermic character for all thermal steps [37].

3.8. Spectrophotometric determination of the stoichiometry of the prepared complexes

Stoichiometry of complexes is investigated using the two methods, continuous-variations method, and mole-ratio method. The methods used and the experimental results showed, the stoichiometry of the prepared complexes is 1:1. The detours of the continuous variation method (cf. Fig. 1) showed maximum absorbance at mole fraction X_{ligand} = 0.43 indicating the formation of complexes with metal ion to ligand ratio 1:1. Moreover, the data resulted from applying the molar ratio method confirm these results (cf. Fig. S2) [38].

3.9. Determination of the apparent forming constants of the synthesized complexes

The formation constants (K_f) of the prepared complexes formed in solution were obtained from the spectrophotometric measures

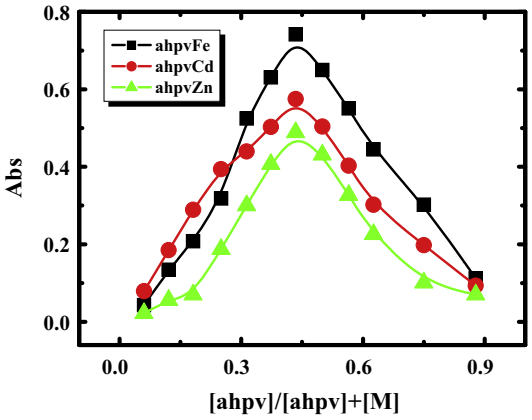

Fig. 1. Continuous variation plots for the prepared complexes in aqueous-alcoholic mixtures at [M] = [ahpv] = 1×10^{-3} M and 298 K.

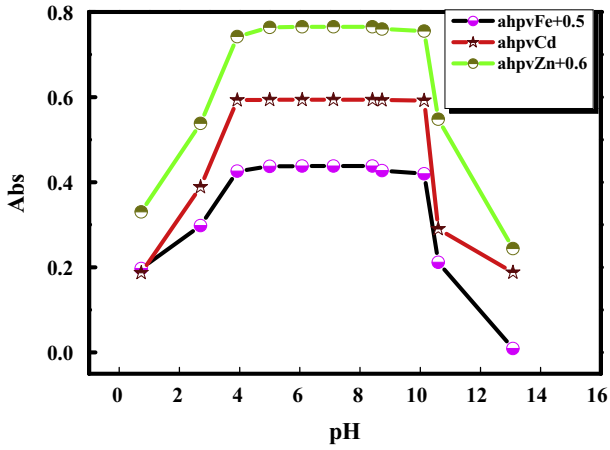

Fig. 2. Dissociation curves of the prepared complexes in aqueous alcohol mixtures at [complex] = 1×10^{-3} M and 298 K.

by applying the continuous variation method [39] (Table 2). The obtained K_f accounts indicate the high stability of the studied complexes. The accounts of K_f for the investigated complexes increase in the following order: ahpvCd > ahpvZn > ahpvFe complex. Moreover, the accounts of the stability constant (pK) and Gibbs free energy ($\Delta G^{\neq}$) of the complexes are evaluated. The negative results of Gibbs free energy mean that the reaction is spontaneous and favorable. The pH-profile presented in (cf. Fig. 2) displayed dissociation curves and a great stability pH range (4–10) of the prepared complexes. This means that the preparation of the complex widely stabilizes the Schiff base. Consequently, the suitable pH range for the various applications of the complexes is from pH = 4 to pH = 10. The results of elemental analysis, molar conductance, magnetic susceptibility, infrared and electronic spectra help to know the structure of the complexes [40].

3.10. Energy-dispersive X-ray spectroscopy (EDX) pattern of the prepared metal oxides

The electron dispersive spectroscopy (EDS) analysis of Fe_2O_3 indicates the presence of Fe and O composition in the pure grown iron oxide NPs (Fe_2O_3). It is clearly displayed that grown synthesize materials contained only iron and oxygen elements, which presented in Fig. 3a. The composition of iron and oxygen is 63.31% and 36.69%, respectively. No other peak related with any impurity has been detected in the EDS, which confirms that the grown NPs are composed only with iron and oxygen. The electron dispersive spectroscopy (EDS) analysis of CdO indicates the presence of Cd and O composition in the pure grown cadmium oxide NPs (CdO). It is clearly displayed that grown synthesize materials contained only cadmium and oxygen elements, which presented in Fig. 3b. The composition of cadmium and oxygen is 27.74% and 72.26%, respectively. No other peak related with any impurity has been detected in the EDS, which confirms that the grown NPs are composed only with cadmium and oxygen. The electron dispersive spectroscopy (EDS) analysis of ZnO indicates the presence of Zn and O composition in the pure grown zinc oxide NPs (ZnO). It is clearly displayed that grown synthesize materials contained only zinc and oxygen elements, which presented in Fig. 3c. The composition of zinc and oxygen is 41.62% and 58.38%, respectively. No other peak related with any impurity has been detected in the EDS, which confirms that the grown NPs are composed only with zinc and oxygen.

3.11. Particle size of the prepared complexes and metal oxides

The Fe(II), Cd(II) and Zn(II) oxides nanoparticles were synthesized at 500 °C using Schiff base complexes as precursors and their properties studied with the assistance of a transmission electron microscope (TEM) and X-ray diffraction. Based on TEM images and the calculated histogram (cf. Figs. 4(a)–(f) and 5(a)–(f)), it is clear that the prepared complexes have particle size of 12 nm, 23 nm and 36 nm for Fe(II), Cd(II) and Zn(II) complexes respectively. It is observed that the complexes have a particle size of 8 nm, 17 nm and 4 nm for nano-sized Fe_2O_3, CdO and ZnO oxides respectively. These conclusions showed that the prepared compounds have a high surface area and this can lead to many important catalytic and potential properties [41]. Fig. 6 demonstrates the XRD patterns of the synthesized Fe_2O_3, CdO and ZnO nanoparticles. The X-ray diffraction data were logged by using Cu Kα radiation (1.5406 Å). The intensity data was gathered over a 2θ range of 5–80°. The medium grain size of the samples was estimated with the help of the Scherrer equation, profiting the diffraction intensity peak. X-ray diffraction studies confirmed that the synthesized materials were Fe_2O_3, CdO and ZnO, that all the diffraction peaks agreed with the reported standard data; no characteristic peaks were denounced other than oxide, MO. The mean grain size (D) of the particles was estimated from the XRD line broadening mensuration using the Scherrer Equation [41,42]:

$$D = 0.89\lambda/\beta\cos\theta \quad (7)$$

where λ is the wavelength (Cu Kα), β is the entire breadth at the half-maximum (FWHM) of the Fe_2O_3, CdO and ZnO line and θ is the diffraction angle. An estimated line broadening of the diffraction

Table 2
The formation constant (K_f), stability constant (pK) and Gibbs free energy ($\Delta G^{\neq}$) values of the synthesized complexes in aqueous-ethanol at 298 K.

Complex	Type of complex	K_f	pK	$\Delta G^{\neq}$ (kJ mol^{-1})
ahpvFe	1:1	4.80×10^9	9.68	−55.20
ahpvCd	1:1	3.41×10^{11}	11.53	−65.76
ahpvZn	1:1	4.81×10^9	9.68	−55.20

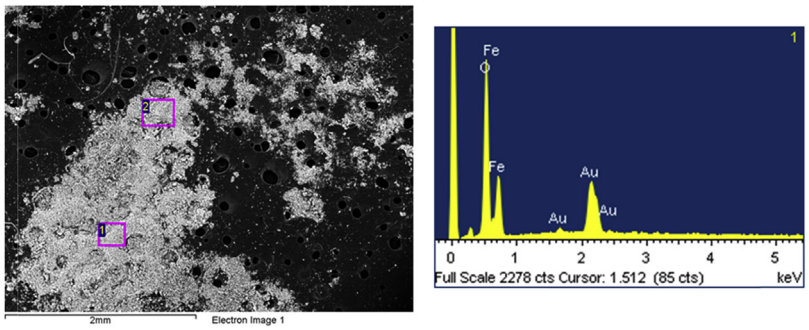

Processing option : All elements analysed (Normalised)

Spectrum	O	Fe
1	36.69	63.31

All results in weight%

(a)

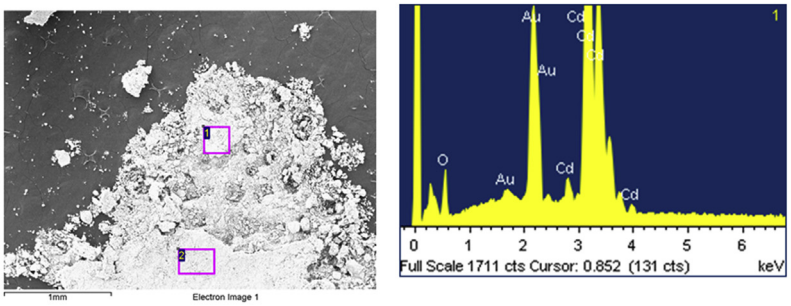

Processing option : All elements analysed (Normalised)

Spectrum	O	Cd
Mean	72.26	27.74

All results in atomic%

(b)

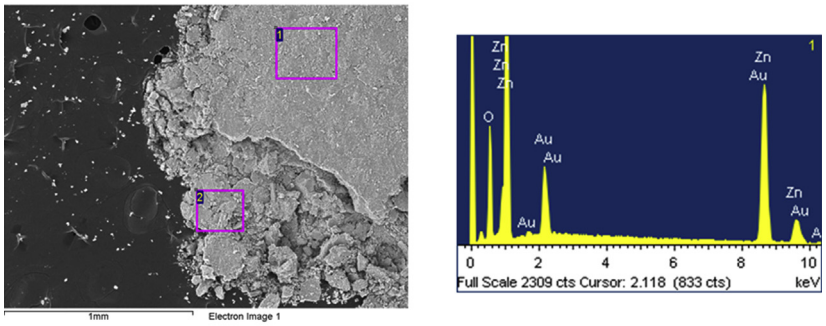

Processing option : All elements analysed (Normalised)

Spectrum	O	Zn
Mean	58.16	41.84

All results in atomic%

(c)

Fig. 3. (a)EDX pattern of Fe_2O_3 nanoparticles. (b) EDX pattern of CdO nanoparticles. (c) EDX pattern of ZnO nanoparticles.

peaks is a caption that the synthesized materials are in the nanometer range. The reaction temperature highly affects the particle morphology of as-prepared Fe_2O_3, CdO and ZnO powders. The finding of nanoparticle size mensuration of samples by XRD and TEM elucidate that the size of the Fe_2O_3, CdO and ZnO nanoparticles was about 4–17 nm.

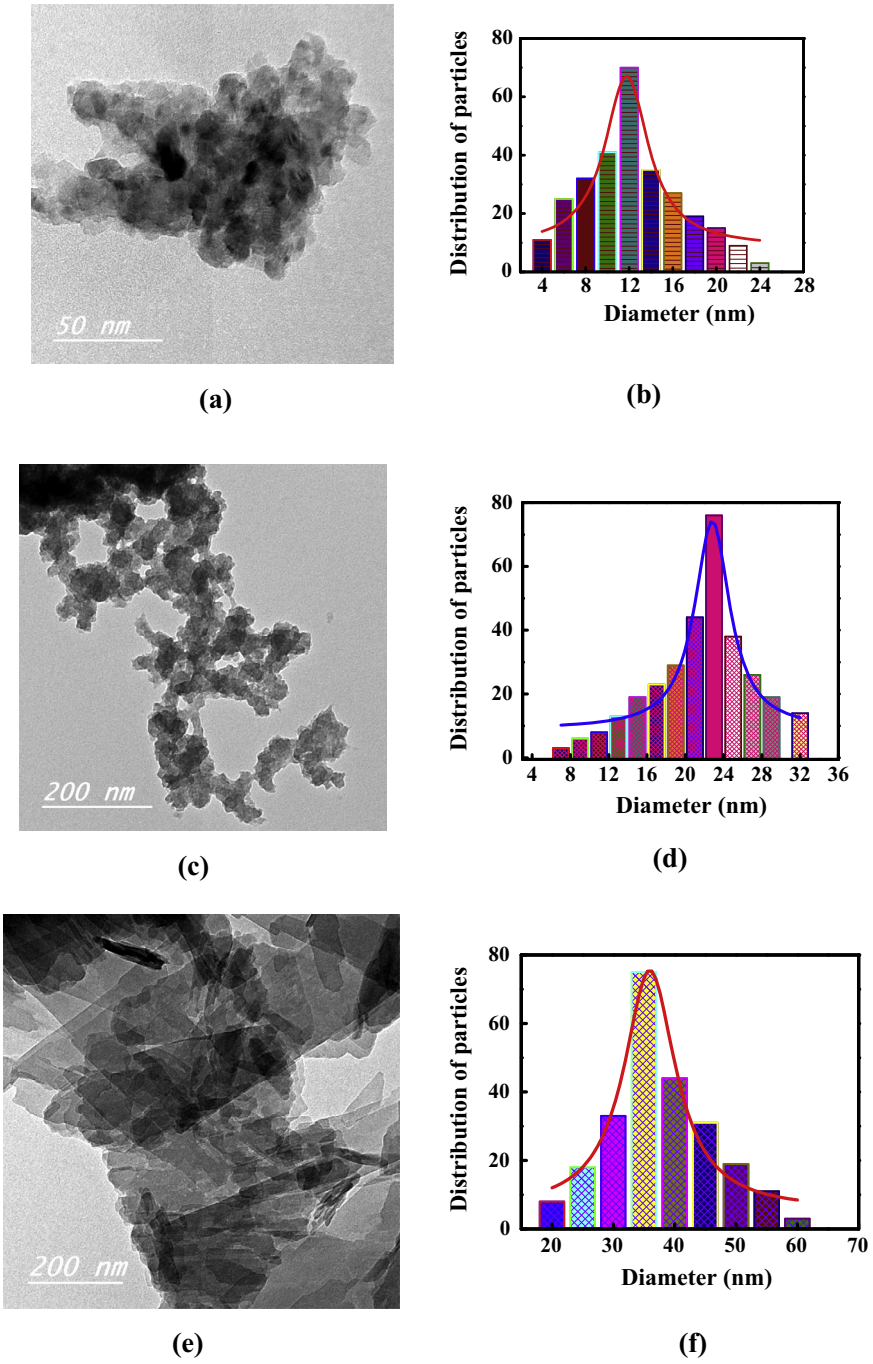

Fig. 4. (a) TEM image of the prepared ahpvFe complex. (b) Calculated histogram for particle size distribution of ahpvFe complex. (c) TEM image of the prepared ahpvCd complex. (d) Calculated histogram for particle size distribution of ahpvCd complex. (e) TEM image of the prepared ahpvZn complex. (f) Calculated histogram for particle size distribution of ahpvZn complex.

3.12. Antimicrobial activity

The *in vitro* antimicrobial actions of the Schiff base ligand, its complexes and their metal oxides against three selected bacteria *(Escherichia coli, Micrococus luteus* and *Serratia marcescence*) and three fungi (*Aspergillus flavus, Getrichm candidum and Fusarium oxysporum)*, were determined. Any chemotherapeutic agent inhibits the growth of microbes by microstatic mechanisms. All of the compounds displayed good biological activity with the micro-organism. On contrasting the biological wares of the Schiff base ligand, its complexes and their metal oxides with those of a standard bactericide and fungicide, it was clear that the complexes had moderate activity as matched with the standard, but all the complexes were more active than free ligand. The nano sized metal oxides have the highest activity. The higher inhibition zone of the transition metal complexes than those of the ligand can be shown based on the Overtone notion and the chelation theory. Upon chelation, the polarity of the metal ion is decreased to a great extent due to the overlap of the ligand orbital and the fractional participating of the positive charge of the metal ion with donor groups. Furthermore, it raises the delocalization of the π-electrons over the whole chelating ring and increases the breakthrough of the complexes into lipid membranes and the blocking of the metal attachment locations in the enzymes of

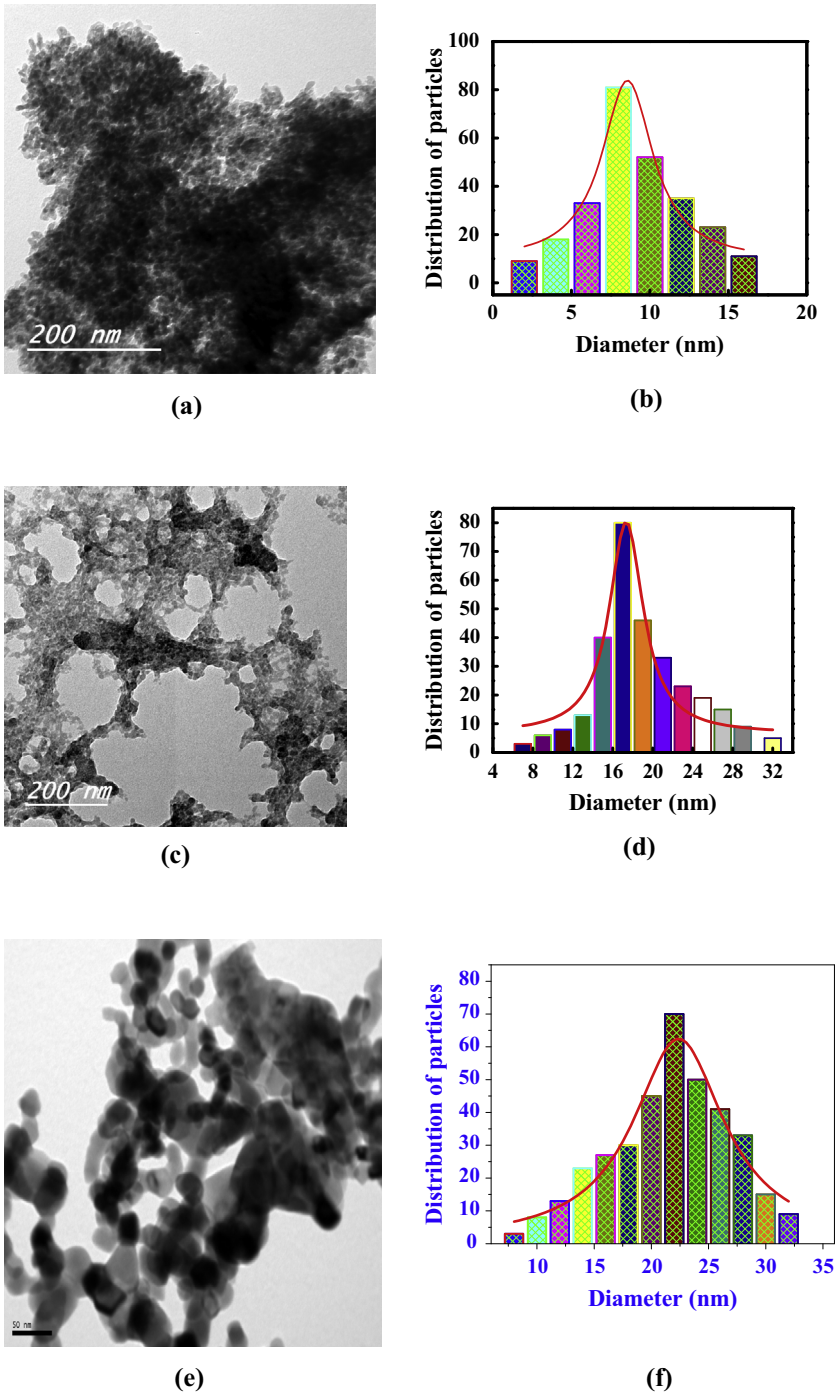

Fig. 5. (a) TEM image of the prepared Fe_2O_3. (b) Calculated histogram for particle size distribution of Fe_2O_3. (c) TEM image of the prepared CdO. (d) Calculated histogram for particle size distribution of CdO. (e) TEM image of the prepared ZnO. (f) Calculated histogram for particle size distribution of ZnO.

micro-organisms [43–46]. The conclusions of the investigations account for the antipathogenic manner of the compounds and this efficacy is positively changed on complexation. Data are listed in Tables (S4, S5) and Figs. 7 and 8. It is shown that antimicrobial potency of metal oxides is better than that of their Schiff base complexes. This could be simply demonstrated as smaller particles normally have a larger surface to volume ratio which offers a more efficient mean for antibacterial activities [47]. The minimum inhibitory concentration (MIC) was estimated by serial dilution route and reported in (cf. Table 3). Among complexes, ahpvFe (3 mg/ml) showed the lowest MIC against *Serratia marcescence*. The ahpvFe complex (2 mg/ml) was found to be lowest MIC against *Escherichia coli*. In the case of *Micrococcus luteus*, the ahpvCd complex (2 mg/ml) showed the lowest MIC. The ahpvFe complex (4 mg/ml) was found to be lowest MIC against *Fusarium oxysporum*. In the case of *Getrichm candidum*, ahpvFe and ahpvCd complexes (2 mg/ml) showed the lowest MIC. The ahpvZn complex (3 mg/ml) was found to be highly effective as they exhibit the lowest MIC against *Aspergillus flavus*. The antimicrobial studies suggested that all the complexes showed significantly enhanced antimicrobial activity against microbial strains in comparison to the free ligands. Previous studies elsewhere suggested that

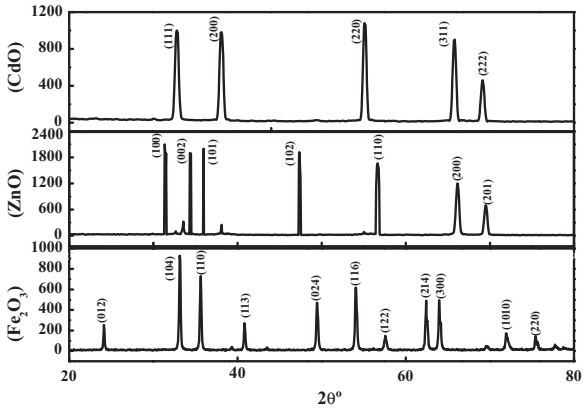

Fig. 6. XRD patterns of Fe_2O_3, CdO and ZnO nanoparticles.

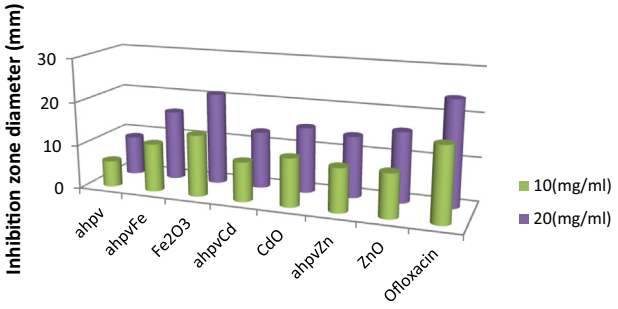

Fig. 7. Zone of inhibition against *Escherichia coli* (bacteria) by the prepared complexes and their metal metal oxides.

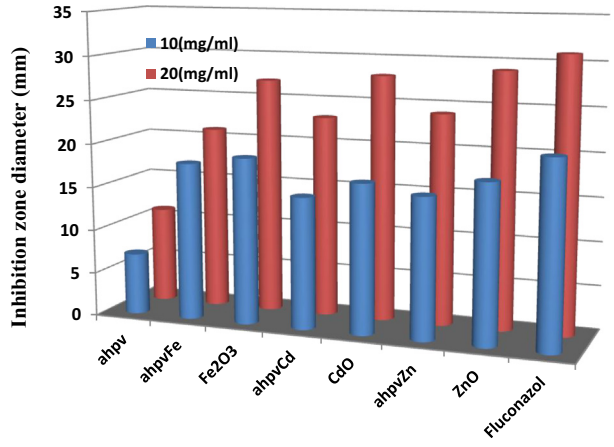

Fig. 8. Zone of inhibition against *Fusarium oxysporum* (fungi) by the prepared complexes and their metal oxides.

chelation tended to make the ligands act as more powerful and potent bactereostatic agents [48], thus inhibited the growth of microbe more than the parent ligands did and it is similar with that of this study. It was suspected that factors such as solubility, conductivity, dipole moment, and cell permeability mechanism influenced by the existence of metal ion might be the possible reason for the increase in activity. The activities of the prepared complexes were confirmed by calculating the potency index (cf. Table 4) according to the following relation [48]:

$$\text{Activity index (A)} = \frac{\text{inhibition zone of complex (mm)}}{\text{inhibition zone of standard drug (mm)}} \times 100 \quad (8)$$

3.13. DNA binding potency

3.13.1. Electronic spectra of interaction with DNA

Titration with electronic absorption spectroscopy is an active route to check the binding mode of DNA with metal complexes. The spectra were registered as a function of the addition of the buffer solutions of pretreated CT-DNA to the buffer solutions of the tested complexes. If the interaction mode is intercalation, the orbital of the intercalated ligand can couple with the orbital of the base pairs, lowering the π–π^* transition energy and lead to bathochromism. If the conjunction orbital is partially filled by electrons, it results in reducing the transition probabilities and lead to hypochromism [49]. The extent of the hypochromism or hyperchromism in the metal-to-ligand charge transfer (MLCT) band is commonly consistent with the force of intercalation interaction [50]. The electronic absorption spectra of ahpvFe complex in the absence and presence of various concentrations of buffered CT-DNA are given in Fig. S3. Addition of increasing amounts of CT-DNA resulted in a reduction of absorbance for a complex. The spectral parameters for the DNA interaction with the tested complexes are shown in Table 5. The investigated complexes could bind to DNA via an intercalative mode with the sequence: ahpvFe > ahpvZn > ahpvCd complex.

3.13.2. Viscosity measurements

For explaining the interaction nature between the tested complexes and DNA, viscosity measures were carried out. Hydrodynamic methods such as viscosity measures which are sensitive to length increment or reduce of DNA are regarded as the most effective routes of studying the binding mode of compounds to DNA in the absence of crystallographic structural data and NMR. For further explaining of the binding mode, viscosity measurements were made. Under appropriate conditions, a traditional intercalative mode such as intercalation of drugs like ethidium bromide leads to a significant increment in the viscosity of DNA solution due to an increment in the segregation of base pairs at the intercalation site and hence an increment in the overall DNA length. On other hand, drug molecules attachment exclusively to the DNA grooves lead to less pronounced in DNA solution viscosity [51] a partial intercalation of compound may bend the DNA helix, resulting in the reduction of its effective length and, concomitantly, its viscosity [52]. The relative viscosity of DNA solution enhances significantly as the amount of the compound raises, as shown in (Fig. 9). This may be due to the admission of the aromatic ring in

Table 3
Results of minimum inhibition concentration (MIC) of the prepared Schiff base ligand and its complexes against different strains of bacteria and fungi.

Compounds	Minimum inhibition concentration (MIC)					
	Serratia Marcescence	*Escherichia coli*	*Micrococcus Luteus*	*Fusarium oxysporum*	*Getrichm candidum*	*Aspergillus flavus*
ahpv	8	6	4	8	13	8
ahpvFe	3	2	5	4	2	5
ahpvCd	4	4	2	7	2	4
ahpvZn	6	7	3	7	5	3

Table 4
Results of activity index % of the prepared Schiff base ligand and its complexes against different strains of bacteria and fungi.

Compounds	Activity index %					
	Serratia Marcescence	*Escherichia coli*	*Micrococcus Luteus*	*Fusarium oxysporum*	*Getrichm candidum*	*Aspergillus flavus*
ahpv	39.3	40.9	38.5	37.5	38.4	35.4
ahpvFe	78.6	72.7	87.2	66.6	87.1	67.7
ahpvCd	71.4	59.1	71.8	54.1	71.1	74.1
ahpvZn	64.3	63.6	79.5	58.3	79.4	77.4

Table 5
Spectral parameters for DNA interaction with the synthesized complexes.

Complex	λ_{max} Free (nm)	λ_{max} Bound (nm)	Δn (nm)	Chromism (%)[a]	Type of chromism	Binding constant $K_b \times 10^6$ mol^{-1} dm^3	$\Delta G^{\neq}$ (kJ mol^{-1})
$[Fe(ahpv)(H_2O)_3]\cdot H_2O$	531	526	5	36.3	Hyper	0.01 ± 0.02	−22.80
	414	419	5	32	Hypo		
$[Cd(ahpv)(H_2O)_3]\cdot H_2O$	393	390	3	19.6	Hypo	0.32 ± 0.02	−31.40
	315	314	1	21.4	Hypo		
$[Zn(ahpv)(H_2O)_3]\cdot 4H_2O$	449	466	17	89.6	Hypo	0.19 ± 0.02	−30.09
	293	353	40	22.6	Hypo		

[a] Chromism (%) = $[(Abs_{free} - Abs_{bound})/Abs_{free}]$.

Schiff base into the DNA base pairs resulting in a crook in the DNA helix, hence, increase in the segregation of the base pairs at the intercalation place and increment in DNA molecular length. Moreover, the sequence of the observed increment in the values of viscosity was renovated with the binding affinity to DNA i.e. ahpvFe complex shows the highest binding affinity to DNA and the highest viscosity.

3.13.3. Gel electrophoresis

Agarose gel electrophoresis is used for the DNA binding studies. The Schiff base Fe(II), Cd(II) and Zn(II) complexes were studied for their DNA binding activity by agarose gel electrophoresis method (Fig. 10). The gel after electrophoresis clearly showed that the intensity of all the treated DNA samples has partially detracted, possibly because of the interaction with DNA. The partial binding of DNA was observed in Fe(II), Cd(II) and Zn(II) complexes of the Schiff base. The difference was clarified in the bands of the complexes compared to that of the control DNA. This explains that the control DNA alone does not show any visible cleavage whereas the complexes show cleavage [53]. However, the nature of reactive intermediates involved in the DNA binding by the complexes is not obvious [54]. These results show that the metal ions play an important role in the interaction with isolated DNA. As the compound

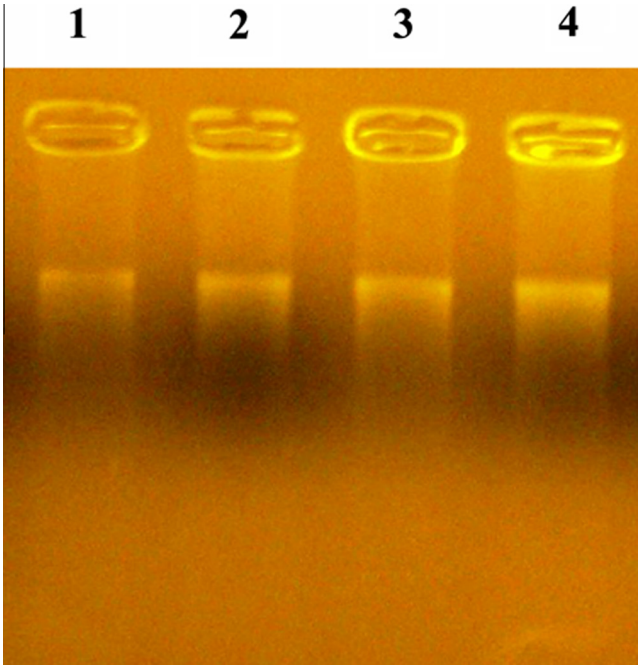

Fig. 10. DNA binding study Calf-thymus (CT)-DNA with Fe(II), Cd(II) and Zn(II) complexes. Lane 1: Fe(II); Lane 2: Zn(II); Lane 3: Cd(II); Lane 4: Control DNA.

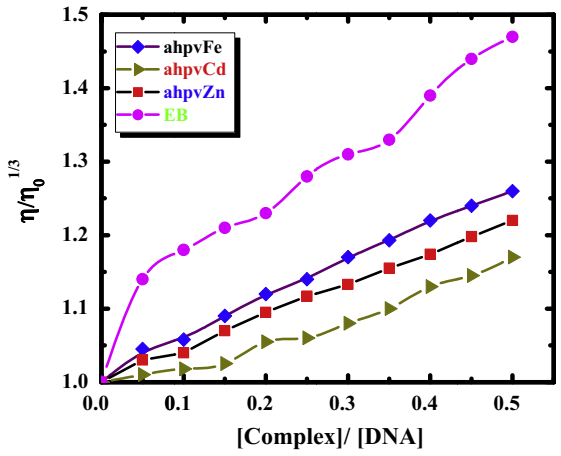

Fig. 9. The effect of increasing the amount of the synthesized complexes on the relative viscosities of DNA at [DNA] = 50 μM, [complex] = 10–60 μM and 298 K.

was observed to bind with DNA, it can be concluded that the compound reduces the growth of the pathogenic organism by interaction with genome. The studies reveal that partial binding of DNA was observed by Fe(II), Cd(II) and Zn(II) complexes. The experimental results indicated that the investigated complexes could bind to DNA via intercalative mode.

3.13.4. Anticancer activity

The cytotoxic potency of Schiff base complexes (2), (3) and (4) was evaluated against colon carcinoma cells, (HCT-116 cell line) and hepatic cellular carcinoma cells, (HepG-2) within 0–10 μM concentration range. The IC_{50} values were evaluated for each compound and results are offered in Fig. 11 and Table S6. As shown, most complexes displayed manifestly cytotoxic potencies (which are greater than that of ligand) compared to vinblastine

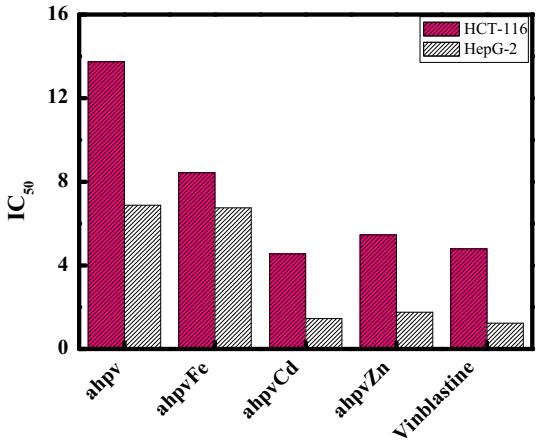

Fig. 11. IC_{50} values of the ahpv ligand and its metal complexes against human Colon carcinoma cells, (HCT-116 cell line) and hepatic cellular carcinoma cells, (HepG-2).

standard drug. It seems that changing the complexation locations and the nature of the metal ion has impact on the biological way. Cytotoxicity potency of the complexes may be due to the focal metal atom which was presented by Tweedy's chelation theory [55]. Cytotoxicity conclusions indicated that all tested complexes (IC_{50} = 4.55–8.44 μg/μl) demonstrated potent cytotoxicity against HCT-116 cancer cells and (IC_{50} = 1.45–6.75 μg/μl) demonstrated potent cytotoxicity against HepG-2 cancer cells. cadmium complex (3) showed the highest cytotoxicity effect with IC_{50} value of 4.55 μg/μl, followed by complex (4) with IC_{50} value 5.46 μg/μl and then complex (2) with IC_{50} value 8.44 μg/μl in case of HCT-116 cancer cells. Cadmium complex (3) showed the highest cytotoxicity effect with IC_{50} value of 1.45 μg/μl, followed by complex (4) with IC_{50} value 1.76 μg/μl and then complex (2) with IC_{50} value 6.75 μg/μl in case of HepG-2 cancer cells It was spotted also that all complexes are more potent than the free ligand. This indicated beneficent of the antitumor potency upon coordination. The refinement of cytotoxic potency may be specified to that the positive charge of the metal increased the acidity of coordinated ligand that bears protons, causing more potent hydrogen bonds which enhanced the biological activity [56]. It seems that changing the coordination locations and the nature of the metal ion has a clear effect on the biological manner by modifying the binding ability of DNA [57]. Gaetke and Chow had reported that metal has been suggested to smooth oxidative tissue damage through a free-radical mediated trajectory analogous to the Fenton reaction [58].

4. Conclusion

Some New nano-sized Fe(II), Cd(II) and Zn(II) Schiff base complexes were synthesized sonochemichally and characterized using different analytical tools. The obtained results showed the existence of one metal ion per one ligand molecule and suggested structure for the complexes $[M(ahpv)(H_2O)_3]\cdot nH_2O$ for Fe(II) and Cd(II) complexes. The electronic spectral data is in favor of an octahedral geometry of the complexes except Zn(II) complex is tetrahedral. The ligand and its Fe(II), Cd(II) and Zn(II) complexes were tested for antimicrobial activity against some pathogens. All the compounds were found to be more active against the bacteria *and* fungi, whereas the ligand displayed the least antimicrobial activity against the bacteria *and* fungi. Moreover, DNA interaction of these compounds was tested by utilizing gel electrophoresis, electronic spectra and viscosity mensurations. The experimental results showed that the complexes could bind to DNA via intercalative mode. Furthermore, nano-sized metal oxides were prepared from their complexes and their antimicrobial activity was evaluated. Very good cytotoxic activity of the selected complexes was found with colon carcinoma cells, (HCT-116 cell line) and hepatic cellular carcinoma cells, (HepG-2).

Appendix A. Supplementary material

Supplementary data associated with this article can be found, in the online version, at http://dx.doi.org/10.1016/j.bioorg.2016.10.009.

References

[1] (a) S. Arulmurugan, Helen P. Kavitha, B.R. Venkatraman, Rasayan J. Chem. 3 (2010) 385–410;
(b) A.M. Abu-Dief, M.S.M. Abdelbaky, S. Garcia-Granda, Acta Cryst. E 72 (2015) 496–497.
[2] A. Prakash, M.P. Gangwar, K.K. Singh, J. Develop. Biol. Tissue Eng. 3 (2011) 13.
[3] K.C. Gupta, A. Kumar Sutar, Coord. Chem. Rev. 252 (2008) 1420.
[4] J. Manna, G. Begum, K. Pranay Kumar, S. Misra, R.K. Rana, ACS Appl. Mater. Interf. 5 (2013) 4457–4463.
[5] B.L. Vallee, D.S. Auld, Acc. Chem. Res. 26 (1993) 543–551.
[6] X.X. Sun, C.M. Qi, S.L. Ma, H.B. Huang, W.X. Zhu, Y.C. Liu, Inorg. Chem. Commun. 9 (2006) 911–914.
[7] J.N. Le Pag, W. Lindner, G. Davies, D.E. Seitz, B.L. Karger, Anal. Chem. 51 (1979) 433–435.
[8] G.K. Mor, K. Shankar, M. Paulose, Nano Lett. 5 (2005) 191–195.
[9] D. Pathania, G. Sharma, R. Thakur, Chem. Eng. J. 267 (2015). 235–244, 550.
[10] C.J. Frederickson, J.Y. Koh, A.I. Bush, Nat. Rev. Neurosci. 6 (2005) 449.
[11] H.T.S. Britton, Hydrogen Ions, third ed., Chapman and Hall, London, UK, 1952.
[12] Disha Tilala, Hardik Gohel, Vishwa Dhinoj, Denish Kari, Int. J. Chem. Tech. Res. 5 (2013) 2330.
[13] A.W. Bauer, W.M. Kirby, J.C. Scherris, M. Truck, Am. J. Clin. Pathol. 45 (1966) 493–496.
[14] L.H. Abdel-Rahman, R.M. El-Khatib, L.A.E. Nassr, A.M. Abu-Dief, F. El-Din Lashin, Spectrochim. Acta Part A: Mol. Biomol., Spectrosc. 111 (2013) 266–276.
[15] L.H. Abdel-Rahman, R.M. El-Khatib, L.A.E. Nassr, A.M. Abu-Dief, Russ. J. Gen. Chem. 84 (2014) 1830–1836.
[16] D. Sabolova, M. Kozurkova, T. Plichta, Z. Ondrusova, D. Hudecova, M. Simkovic, H. Paulıkova, A. Valent, Int. J. Bio. Macromol. 48 (2011) 319–325.
[17] L.H. Abdel-Rahman, R.M. El-Khatib, L.A.E. Nassr, Ahmed M. Abu-Dief, M. Ismail, A.A. Seleem, Spectrochim. Acta Part A Mol. Biomol. Spectrosc. 117 (2014) 366.
[18] N. Raman et al., J. Chem. Sci. 119 (2007) 303–310.
[19] S.S. Hindo, M. Frezza, D. Tomco, M.J. Heeg, L. Hryhorczuk, B.R. McGarvey, Q.P. Dou, C.N. Verani, Eur. J. Med. Chem. 44 (2009) 4353–4361.
[20] M.I. Hossain, M. Switalska, W. Peng, M. Takashima, N. Wang, M. Kaiser, J. Wietrzyk, S. Dan, T. Yamori, T. Inokuchi, Eur. J. Med. Chem. 69 (2013) 294–309.
[21] L.H. Abdel-Rahman, A.M. Abu-Dief, R.M. El-Khatib, S.M. Abdel-Fatah, J. Photochem. Photobiol. B 162 (2016) 298–308.
[22] L.H. Abdel-Rahman, A.M. Abu-Dief, M.S.S. Adam, S.K. Hamdan, Catal. Lett. 146 (2016) 1373–1396.
[23] Y.-Z. Cui, Y. Yuan, Z.-F. Li, M. Liu, Q.-H. Jin, N. Jiang, L.-N. Cui, S. Gao, Polyhedron 112 (2016) 118–129.
[24] A.M. Abu-Dief, R. Díaz-Torres, E.C. Sañudo, L.H. Abdel-Rahman, N.A. Alcalde, Polyhedron 64 (2013) 203–208.
[25] M.M. Omar, G.G. Mohammed, Spectrochim. Acta A 61 (2005) 929.
[26] A.P. Mishra, R.K. Mishra, S.P. Shrivastava, J. Serb. Chem. Soc. 74 (2009) 523.
[27] M.A. Neelakantan, S.S. Marriappan, J. Dharmaraja, T. Jeyakumar, K. Muthukumaran, Spectrochim. Acta A 71 (2008) 628.
[28] S. Samadhiya, A. Halve, Orient. J. Chem. 17 (2001) 119.
[29] F. Ahmad, M. Parvez, S. Ali, M. Mazhar, A. Munir, Synth. React. Inorg. Met. Org. Chem. 32 (2002) 665–687.
[30] D.X. West, A.A. Nasar, Trans. Met. Chem. 24 (1999) 617–621.
[31] L.H. Abdel-Rahman, A.M. Abu-Dief, M.A. Ismael, M.A. Mohamed, N.A. Hashem, J. Mol. Struct. 1103 (2016) 232–244.
[32] E. Canpolat, M. Kaya, J. Coord. Chem. 55 (2002) 961–968.
[33] Feng Gao, Wen-Juan Ruan, Jia-Mei Chen, Ying-Hui Zhang, Zhi-Ang Zhu, Spectrochim. Acta Part A Mol. Biomol. Spectrosc. 62 (2005) 886–895.
[34] Jain, Mishra, J. Serb. Chem. Soc. 77 (2012) 1013–1029.
[35] Mohammad Shakir, Summaiya Hanif, Mohd Asif Sherwani, Owais Mohammad, Mohammad Azam, Saud I. Al-Resayes, J. Photochem. Photobiol. B: Biol. 157 (2016) 39–56.
[36] E.-H.M. Diefallah, Thermochim. Acta 202 (1992) 1–16.
[37] Narendra Kumar Chaudhary, Am. J. Appl. Chem. 2 (2014) 19–26.
[38] (a) L.H. Abdel-Rahman, R.M. El-Khatib, L.A.E. Nassr, A.M. Abu-Dief, Int. J. Chem. Kin. A 46 (2014) 543–555;
(b) H.M. Abd El-Lateef, A.M. Abu-Dief, B.E.M. El-Gendy, J. Electroanal. Chem. 758 (2015) 135–147.
[39] L.H. Abdel-Rahman, A.M. Abu-Dief, S.K. Hamdan, A.A. Seleem, Int. J. Nano Chim. 1 (2015) 65–77.

[40] A.M. Abu-Dief, L.A.E. Nassr, J. Iran Chem. Soc. 12 (2015) 943–955.
[41] M.A.A.A. El-Remaily, A.M. Abu-Dief, Tetrahedron 71 (2015) 2579–2584.
[42] (a) P. Scherrer, Göttinger Nachrichten Gesell. 2 (1918) 98;
(b) A.M. Abu-Dief, M.S.M. Abdelbakyb, M.S.M. Abdelbakyb, D. Martínez-Blanco, Z. Amghouz, S. García-Granda, Mater. Chem. Phys. 174 (2016) 164–171.
[43] Z.H. Chohan, H. Pervez, A. Rauf, K.M. Khan, C.T. Supuran, J. Enzym. Inhib. Med. Chem. 39 (2004) 417.
[44] Z.H. Chohan, Met.-Based Drugs 6 (1999) 75.
[45] R.R. Coombs, S.A. Westcott, A. Decken, F.J. Baerlocher, Transition Met. Chem. 30 (2005) 411.
[46] B.G. Tweedy, Phytopathology 55 (1964) 910.
[47] C. Jayaseelana, A. Abdul Rahuman, A. Vishnu Kirthi, S. Marimuthu, T. Santhosh kumara, A. Bagavana, K. Gauravb, L. Karthik, K.V. Bhaskara Raob, Spectrochim. Acta Part A 90 (2012) 78–84.
[48] Zakia Khanam, Chew Shwu Wen, Irshad Ul Haq Bhat, J. King Saud Univ. 27 (2015) 23–30.
[49] A.M. Pyle, J.P. Rehmann, R. Meshoyrer, C.V. Kumar, N.J. Turro, J.K. Barton, J. Am. Chem. Soc. 111 (1989) 3051–3058.
[50] X.W. Liu, J. Li, H. Li, K.C. Zheng, H. Chao, L.N. Ji, J. Inorg. Biochem. 99 (2005) 2372–2380.
[51] S. Shi, J. Liu, J. Li, K.C. Zheng, X.M. Huang, C.P. Tan, L.M. Chen, L.N. Ji, J. Inorg. Biochem. 100 (2006) 385–395.
[52] Y. Liu, W. Mei, J. Lu, H. Zhao, L. He, F. Wu, J. Coord. Chem. 61 (2008) 3213–3224.
[53] Anand Prakash Mishra, Herhita Purwar, Rajendra Kumar Jain, Biointerface Res. 2 (2012) 291–299.
[54] (a) L.H. Abdel Rahman, A.M. Abu-Dief, N.A. Hashem, A.A. Seleem, Int. J. Nano Chem. 1 (2015) 79–95;
(b) L.H. Abdel-Rahman, R.M. El-Khatib, L.A.E. Nassr, A.M. Abu-Dief, J. Mol. Struct. 1040 (2013) 9.
[55] (a) B. Tweedy, Phytopathology 55 (1964) 910–914;
(b) L.H. Abdel-Rahman, R.M. El-Khatib, A.M. Abu-Dief, S.M. Abdel-Fatah, A.A. Sleem, Int. J. Nano Chem. 2 (2016) 83–91.
[56] G. Feng, J.C. Mareque-Rivas, N.H. Williams, Chem. Commun. 17 (2006) 1845–1847.
[57] L.H. Abdel-Rahman, A.M. Abu-Dief, E.F. Newair, S.K. Hamdan, J. Photochem. Photobiol. B 160 (2016) 18–31.
[58] L.M. Gaetke, C.K. Chow, Toxicology 189 (2003) 147–163.